Finite-temperature phonon dispersion and vibrational dynamics of BaTiO₃ from first-principles molecular dynamics

Xiaohan Zhang [1], Chunyi Zhang,[2] Cui Zhang,[3] Ping Zhang,[4,2] and Wei Kang [2,*]

[1]*HEDPS, Center for Applied Physics and Technology and School of Physics, Peking University, Beijing 100871, China*
[2]*HEDPS, Center for Applied Physics and Technology and College of Engineering, Peking University, Beijing 100871, China*
[3]*Institute of Physics, Chinese Academy of Sciences, Beijing 100190, China*
[4]*Institute of Applied Physics and Computational Mathematics, Beijing 100088, China*

A systematic investigation of the finite-temperature phonon dispersion, including its smearing and temperature effects, is carried out using autocorrelation function method together with first-principles molecular dynamics method along the [001] direction of BaTiO₃, as an illustrating example of entropy-stabilized structures. A unique anharmonicity in the cubic phase mainly derived from the interactions between titanium and oxygen atoms is revealed, which provides extremely strong damping and smearing to longitudinal optical phonons but no discernible effect on the shift of phonon energies. The anharmonicity gives rise to a nearly constant density distribution in a cubic region around the equilibrium position of the relative motion of titanium atoms with respect to oxygen atoms. These results may help to gain a further insight into complex interactions in entropy-stabilized structures and provide an essential benchmark reference to the development of the promising machine-learning based molecular dynamics methods for the investigation of phonon properties.

I. INTRODUCTION

Vibrational motion of ions is one of the fundamental properties of solids [1,2]. It not only accounts for basic thermal and structural properties of solids such as thermal expansion [3], heat capacity [4], phase transitions [2], bonding length, and angles [4], but also has a close relation to a variety of extraordinary phenomena, e.g., thermoelectricity [5], superconductivity [6,7], and ferroelectricity [8]. Theoretical prediction of the vibrational motion (usually viewed as a superposition of its normal modes—phonons) for its various aspects, e.g., dispersion relation and smearing of phonons [9], infrared spectra [10], Raman spectra [11], and scattering properties with respect to neutron [12] or x ray [13], is thus of persisting interests to the related fields.

Considering the ionic motion as a small vibrational perturbation around the equilibrium position of ions is usually taken as the starting point of present phonon theory [2], which affords a sophisticate description to ionic motions under a broad range of conditions [9]. Practical implementations of this idea, e.g., the frozen-phonon method [14,15] and the density functional perturbation theory (DFPT) method [16,17], have been successfully applied to metals [18,19], semiconductors [20,21], and nanostructures [22,23]. As long as the equilibrium position of ions is located inside a local well of the potential energy hypersurface, ionic motions may well be described through harmonic or quasiharmonic approximations of phonon [2,4].

However, at relatively high temperatures, the phonon energy may be significantly shifted by anharmonic effects, as has been revealed in simple one-dimensional lattice models [24], high-pressure phases of hydrogen [25,26], and a variety of minerals in the crust of the earth [12,27]. More subtly, when the phase is stabilized with the help of entropy, the equilibrium position can even be located at a local maximum point of the potential hypersurface at zero temperature. This is a typical situation of ferroelectric materials such as BaTiO₃ [28–30] and SrTiO₃ [31,32] in their cubic paraelectric phases. In particular, there have been a long-lasting discussion on the coexistence of displacive and order-disorder transition from the cubic to the tetragonal phases of BaTiO₃ [33–35], which is still an open question attracting recent attention [36–39]. It thus calls for methods of a better description for the ionic motion at finite temperature.

A possible option is to extract the information of phonon excitation from the autocorrelation function of ionic velocities [40,41]. This approach connects the Fourier transform of velocity autocorrelation function to the spectrum of one-phonon energy intensity [40,41], which naturally contains the information of phonon dispersion relation and smearing. Together with the first-principles molecular dynamics (FPMD) method [42–44], it is thus able to provide a phonon spectrum that can be directly compared with inelastic neutron scattering experiments.

However, because of the great computational costs, the application of the autocorrelation method in conjunction with the FPMD method is still in its early stage. Most of the dispersion curves were calculated using classical models of ionic interaction [41,45–48] or simplified models of electronic structures [49,50]. There have been very limited reports [51] on the calculation of dispersion relation along a certain direction using the autocorrelation method based on FPMD simulations even for simple structures, e.g., the common

*weikang@pku.edu.cn

face-centered cubic structures. For more complex structures, only phonon properties at a few high symmetric points of the Brillouin zone have been studied in this way [52].

In this work, we provide a systematic investigation of the finite-temperature phonon dispersion, including its smearing and temperature effects, along the [001] direction of $BaTiO_3$ using the autocorrelation function of ionic velocities obtained from FPMD simulations. The high-temperature cubic phase of $BaTiO_3$ has a perovskite structure, and it is a typical example of entropy-stabilized complex structures. We find that $BaTiO_3$ has a unique anharmonicity in the cubic phase. It provides an extremely strong scattering mechanism to damp and smear the longitudinal phonons along the [001] direction but no discernible effects on the shift of phonon energies, which is quite unusual since damping of amplitude and shifting of phonon energy generally occur together. The unique anharmonicity mainly comes from the highly nonlinear interaction between titanium (Ti) atoms and oxygen (O) atoms.

Density distribution of Ti atoms relative to O atoms shows that there is an approximately cubic region around the equilibrium position of the Ti-O relative motion in the high-temperature cubic phase. Inside the cube, the average potential hypersurface is quite flat. In addition, calculated acoustic phonon dispersions are found to be in good agreement with experimental measurements [53–55]. However, no transverse optical soft modes are observed along the [001] direction in our calculations, which supports the experimental findings of Harada *et al.* [56] but differs from earlier measurements of Shirane *et al.* [53].

These results may help us to gain further insight into the unique phonon properties of entropy-stabilized materials on one hand. On the other hand, they serve as an essential benchmark reference for the evaluation of the validity and performance of the machine-learning based molecular dynamics method [57], which is to be employed for the investigation of phonon properties in complex materials [58,59].

The paper is organized as follows. In Sec. II, the methodology and simulation details are presented. In Sec. III, we show the results of calculated phonon spectra along the [001] direction and density distributions of Ti with respect to barium (Ba) and O atoms. Finally, a short concluding remark is given in Sec. IV.

II. METHODOLOGY AND COMPUTATIONAL DETAILS

A. Velocity autocorrelation method

An important application of autocorrelation function is to identify repetitive signals [60]. When a physical event repeatedly occurs at a certain frequency or spatial interval with background noises, its autocorrelation function, with respect to time or space, can filter the noises out and highlight the repeated signal. The Fourier transform of the autocorrelation function then shows a corresponding sharp peak at that repeating frequency or wave number. In a thermal excited lattice system, a phonon vibrational mode can be viewed as such a repetitive physical event so that one can find its peak position in the frequency-wave number plane using the autocorrelation function method. The set of all peak positions, which defines the relation between frequency and wave number for all the

phonon modes, then gives the phonon dispersion relation that can be directly compared with experiments. In addition, the width of the peaks at frequency, i.e., the smearing, is considered to be inversely proportional to the lifetime of the phonon modes.

In lattice systems, one is free to choose physical quantities, e.g., velocity or displacement, to represent the repeated physical event. Here, we follow the work of Thomas *et al.* [41] using mass-weighted velocity in the calculation of autocorrelation function, of which the Fourier transform is closely related to the kinetic energy density distribution of the phonon modes [41].

In a simulation system with N unit cells, the equilibrium position of the bth atom at the nth unit cell is denoted as $\boldsymbol{r}\binom{n}{b}$, determined as the average position of the atom during the whole simulation time τ_0. $\boldsymbol{u}\binom{n}{b};t)$ is the displacement of the atom from its equilibrium position at time t. The velocity component of the atom in the αth direction is then written as $\dot{u}_\alpha\binom{n}{b};t)$. The Fourier transform of the weighted autocorrelation function, which is also called the phonon density spectrum Φ, can thus be expressed as

$$\Phi(\boldsymbol{\kappa}, \omega) = \lim_{\tau_0 \to \infty} \frac{1}{4\pi\tau_0 N} \sum_\alpha \sum_b m_b$$

$$\times \left| \int_0^{\tau_0} \sum_n^N \dot{u}_\alpha\binom{n}{b};t) \exp\left[i\boldsymbol{\kappa} \cdot \boldsymbol{r}\binom{n}{b} - i\omega t\right] dt \right|^2,$$

(1)

where $\boldsymbol{\kappa}$ is the wave vector, and ω is the angular frequency. The resolution of angular frequency is $\Delta\omega = \frac{2\pi}{\tau_0}$, and the resolution of wave number along $\boldsymbol{\kappa}$ is $\Delta\kappa = (\frac{2\pi}{a})\frac{1}{N'}$, where a is the length of a unit cell along that direction, and N' is the number of repeated unit cells along the direction.

B. Simulation details

Phonon dispersions of $BaTiO_3$ at several temperatures across the ferroelectric transition temperature T_0, 393 K as determined by experiments [28], are calculated in our investigations, including the dispersions along the [001] direction at 290 K, 473 K, and 758 K. $BaTiO_3$ has different structures across the transition temperature [28]. At 290 K, it is in the ferroelectric phase with a tetragonal primitive cell. But at 473 K and 758 K, it is in the paraelectric phase and has a cubic primitive cell.

The extended calculation cell is constructed as a square prism by repeating the primitive cells. The direction of interest [001] is set along the z axis of the Cartesian coordinates, as displayed in Fig. 1. In order to obtain sufficient resolution in the wave-number space while keeping the computational cost within a affordable range, the number of primitive units along the direction of interest is set to be 12 or more depending on the length of wave vector from the center to the boundary of the Brillouin zone. But the number of repetitive units perpendicular to the calculated direction is kept to a minimum. Note that, because of the periodic boundary conditions employed in the calculation, transverse dynamic correlation effect [61] is significant and may lead to artificial results when
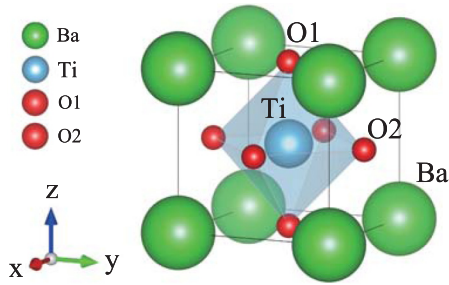
FIG. 1. Schematic illustration of the primitive unit cell of $BaTiO_3$ used in FPMD simulations, where green balls represent Ba, blue ball represents Ti, and red ones are O. The [001] direction in the phonon dispersion calculation is along the z axis of the coordinate system.

the number of repeated units perpendicular to the direction of q is too small. So, in the calculation of dispersions along the [001] direction, the number of repeated primitive cells in the perpendicular direction is set to be 2 along each axis. It turns out to be the minimum requirement to remove dynamic correlation between adjacent primitive cells, as learned from separate trial simulations.

Velocities and displacements of ions used in the velocity autocorrelation method are obtained from the FPMD simulations, carried out using the QUANTUM ESPRESSO package [62]. The electron-ion interaction is represented by pseudopotentials in the projector augmented-wave format [63] with a plane-wave kinetic energy cutoff of 40 Ry. The local density approximation (LDA) [64] functional is employed for the exchange-correlation potential. The time step of simulations is 1.0 fs at 290 K and 473 K and is 0.5 fs at 758 K. The system is first equilibrated at target temperature in a NVT ensemble for 5 ps. Then it is put into a NVE ensemble for at least 60 ps to collect data of atomic velocities and displacements. The long simulation time guarantees the resolution of angular frequency no larger than 0.5 cm^{-1}. All other parameters used in the FPMD simulations are summarized in Table I.

For comparison purposes, we also calculate phonon dispersions for the cubic and tetragonal phases with the DFPT method. The DFPT calculations are performed using the PHonon module [16] in the QUANTUM ESPRESSO package. In the calculation of the cubic phase, the lattice constant is relaxed to 3.9463 Å while the crystal structure remains the $Pm\bar{3}m$ symmetry. The lattice constants are relaxed to $a = 3.9905$ Å and $c = 4.1758$ Å in the tetragonal phase. The coupling between phonons and macroscopic electric fields in the long-wavelength limit is included and crystal acoustic sum rule is enforced.

III. RESULTS AND DISCUSSION

A. Phonon spectra crossing the phase transition

Figure 2 displays phonon spectra in the low-temperature tetragonal phase and high-temperature cubic phase along the [001] direction, where Fig. 2(a) shows phonon spectra of the tetragonal phase at 290 K, and Figs. 2(b) and 2(c) show those of the cubic phase at 473 K and 758 K, respectively. Calculated phonon spectra are plotted as colored contour maps, where the warm color represents high phonon density while the cold color denotes low phonon density. Each phonon branch is given a label according to its polarization and long wavelength behavior in the figure, such as longitudinal (L) acoustic (A), transverse (T) optical (O), LO, and TA phonons. The stair steps observed at the bottom of each spectrum are caused by relatively small size of the calculation cell, which results in a finite resolution along q. As a comparison, the dispersions obtained from DFPT calculations are plotted in Fig. 2 as dashed lines, and results of inelastic neutron scattering experiments [53–55] are displayed as dots. In particular, soft-mode measurements [53] are highlighted with red circles.

A significant feature displayed by the finite-temperature phonon spectra is the strong damping of the LO3 branch across the phase transition. Compared with the LO3 branch in the tetragonal phase in Fig. 2(a), the branches in the cubic phase in Figs. 2(b) and 2(c) appear a remarkable smearing, and the phonon density is much lower than that in the tetragonal phase, indicating a strong scattering. A consequence of this feature is that the LO3 branch is difficult to measure in experiments at high temperatures, as also noticed in previous experiments [55]. Furthermore, the LO1 and LO2 branches display similar trends of damping and smearing as well. However, owing to the influence of nearby TO branches, the features of LO1 and LO2 are not as significant as that of LO3.

There are several common features shared among these three (LO1, LO2, and LO3) phonon branches. First of all, they are all longitudinal optical phonon modes, which are confirmed by decomposing ionic motions into phonon modes (using the methods described in the Appendix) and direct DFPT calculation of the modes at zero temperature. Secondly, the damping and smearing of the three phonon branches across the transition temperature take place at all transfer momentums in the [001] direction, indicating that the scattering induces global fluctuations over the entire Brillouin zone. However, the energies of these phonons in the cubic

TABLE I. Parameters of $BaTiO_3$ in the tetragonal and cubic phases used in the FPMD simulations.

Phase	Tetragonal	Cubic	
T (K)	290	473	758
Latt. param. (Å)	(a) 3.9925 (c) 4.0365 [65]	4.004 [66]	4.0258 [67]
Cell size	$2 \times 2 \times 12$	$2 \times 2 \times 12$	$2 \times 2 \times 12$
k mesh	$2 \times 2 \times 1$	$2 \times 2 \times 1$	$2 \times 2 \times 1$
Time step (fs)	1.0	1.0	0.5
Simulation time (ps)	84	65	80
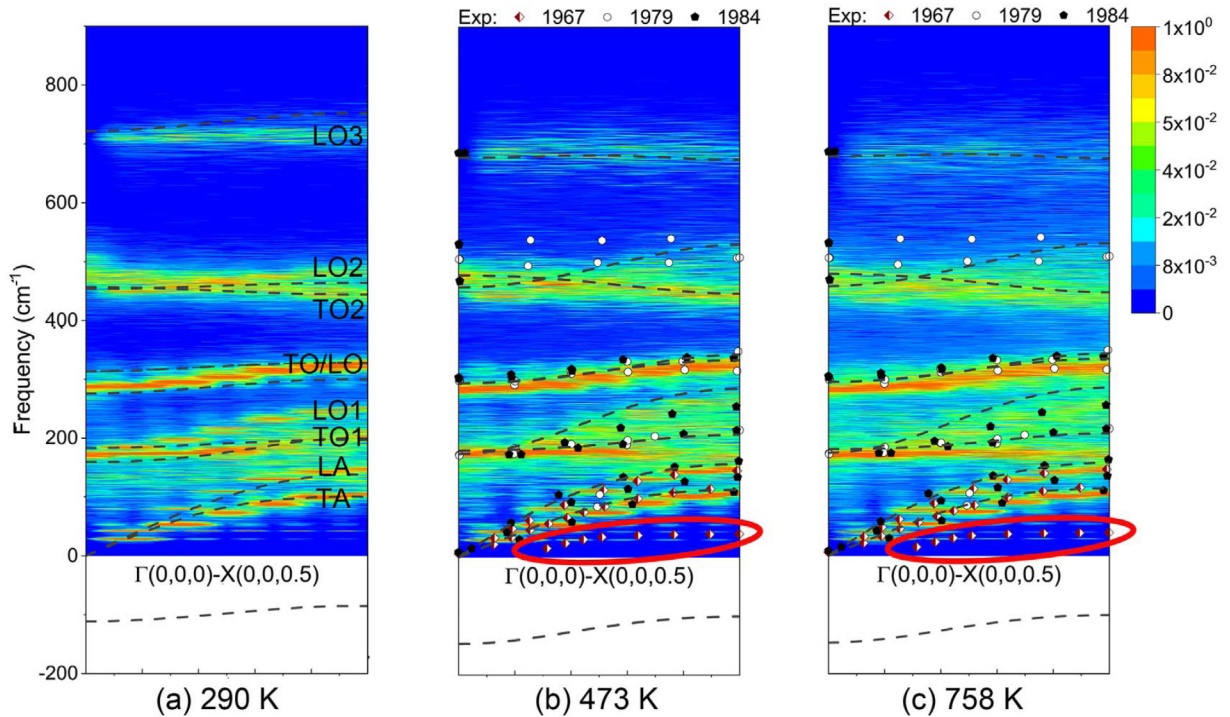
FIG. 2. Phonon spectra at (a) 290 K in the tetragonal phase, (b) 473 K and (c) 758 K in the cubic phase along the [001] direction of the Brillouin zone. Colored maps are finite-temperature phonon spectra calculated using the autocorrelation method, and dashed lines are DFPT results. Inelastic neutron scattering measurements are displayed as dots, where diamonds are taken from the experiment of Shirane *et al.* [53] in 1967, circular dots come from the experiment of Bouillot *et al.* [54] in 1979, and pentagonal dots are the results of the experiment of Jannot *et al.* [55] in 1984.

phase, determined by the peak positions, remain almost the same as those in the low-temperature tetragonal phase. Global fluctuations in phonon modes were considered to be closely associated with order-disorder phase transitions, as pointed out by Zhong *et al.* [68,69]. However, our calculation of dynamical local structures presented in the next subsection show that such global fluctuations are resulted from strong anharmonic effects between ions, which are not necessary coming from double-well interaction potentials. Therefore, the global fluctuation feature may only be a necessary condition for the order-disorder phase transition.

The low-frequency acoustic branches in Fig. 2, featured with clear peaks of high phonon densities, are in good agreement with the experimental results and DFPT calculations. Such agreement effectively verifies the accuracy of phonon spectrum calculations for $BaTiO_3$ using the autocorrelation function method, since the acoustic phonons (with the lowest frequencies) take the longest FPMD trajectory to guarantee the convergence of the results. Below the acoustic branches, there are no clear peaks of soft modes observed in our calculations. These findings are consistent with experimental results of Harada *et al.* [56] but distinct from the soft-mode measurements of Shirane *et al.* [53]. They are also in line with the DFPT calculations, showing that all soft modes have imaginary frequencies, i.e., they are strongly damped phonon modes. To confirm that the imaginary-frequency modes obtained in the DFPT calculation are not stabilized, i.e., the frequency of the mode does not become real, by finite-temperature anharmonic effects in the cubic phase, we project

the velocities at 758 K on the eigenvector of the imaginary mode at the X point of the Brillouin zone following the method of Zhang *et al.* [47]. It shows that the autocorrelation function of the projected velocities does decay exponentially without oscillation.

Anharmonic effects of energy shift at very high temperature, e.g., 758 K, are observed in the transverse optical TO1 branch. The anharmonic shift takes place at the right half of the branch close to the X point of the Brillouin zone. The largest shift is about 30 cm^{-1} at the X point compared with the DFPT dispersion curve. However, it should be noted that, because ions in the FPMD calculation are classical with no nuclear quantum effects included, the temperature at which significant anharmonic shift is observed in experiments should be higher than that predicted by our calculations. For example, at the experimental temperature 473 K, thermal energy is 328 cm^{-1} or 0.0408 eV, which is comparable to the phonon energy about 200 cm^{-1}. Considering a phonon having a Bose-Einstein distribution, this suggests that measured phonon dispersion of the TO1 branch [55], displayed in Fig. 2(b) as dots, at this temperature be closer to the one calculated using the DFPT method at zero temperature, as dashed lines in Fig. 2(b), than that predicted using the velocity autocorrelation method.

In the branches LO2 and TO2 near 470 cm^{-1}, significant differences between calculated spectra and experimental measurements are observed. The phonon energy calculated using the autocorrelation method is generally lower by about 50 cm^{-1} than experimental results. In addition, the
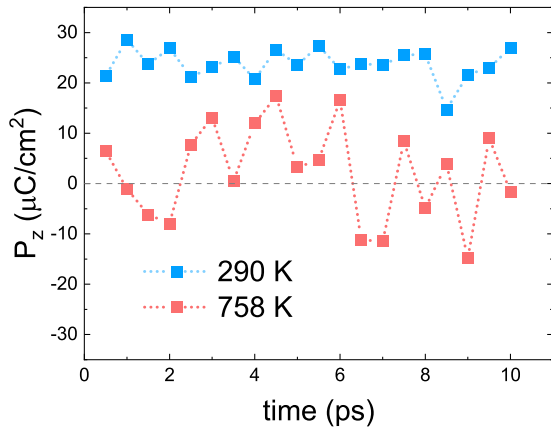
FIG. 3. Instantaneous polarization of $BaTiO_3$ in the ferroelectric phase, 290 K, and in the paraelectric phase, 758 K.

DFPT calculation shows the same underestimation as the autocorrelation function method does, suggesting that the underestimation is not induced by anharmonic effects at finite temperature. This underestimation turns out to be quite general in the density functional theory based calculations [70]. For example, DFPT calculations using Perdew-Burke-Ernzerhof exchange-correlation functional [71] and strongly constrained appropriately normed functional (SCAN) [72] display similar underestimations, as reported in the systematic work of Zhang *et al.* [70]. So, the differences may possibly come from the inaccuracy of exchange-correlation functionals, which has not been addressed by recent developments of exchange-correlation functional models, e.g., the SCAN functional. It will thus be interesting for future experiments to revisit the measurements of phonon modes near 470 cm^{-1}, which should help to gain further insight into the subtle feature of exchange-correlation interaction and the finite-temperature phonon property in systems with complex interaction.

B. Dynamical local structures

We first show that the transition from the high-temperature cubic phase to the low-temperature tetragonal phase is a ferroelectric phase transition by computing the polarization of $BaTiO_3$ at 290 K and 758 K, respectively, along the FPMD trajectories. We choose 20 configurations every 0.5 ps along the trajectories to calculate the dipole moment using the maximally localized Wannier function method [73,74]. The polarization of each configuration is displayed in Fig. 3. At 290 K, the polarization fluctuates between 20–30 $\mu C/cm^2$ with time, implying a ferroelectric phase of $BaTiO_3$. The average of polarization at 290 K is 23.8 $\mu C/cm^2$, consistent with the experimental value 26 $\mu C/cm^2$ [75]. When the temperature is raised to 758 K, the polarization vibrates near zero, which indicates a typical feature of paraelectric phase.

To further reveal the origin of the damping and smearing in the longitudinal optical branches, atomic density distributions of Ti projected along the [001] direction are plotted in Fig. 4 with respect to the position of Ba or O1 atoms. The distributions are extracted from the same FPMD trajectories used to calculate the phonon spectra in Fig. 2. In previous investiga-
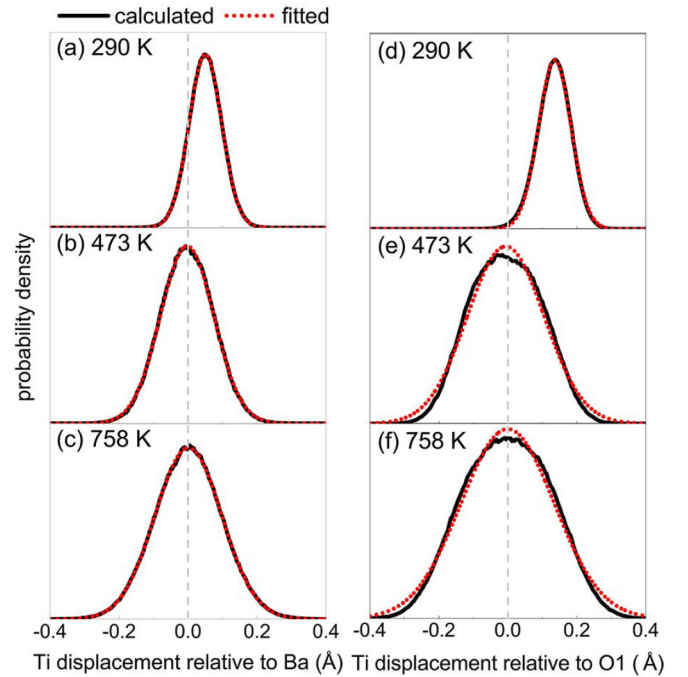
FIG. 4. Density distribution of Ti with respect to Ba and O1 atoms along the [001] direction. (a), (b), and (c) are distributions of Ti relative to Ba. (d), (e), and (f) are distributions of Ti relative to O1.

tions, they were often used to illustrate the anharmonicity of the interaction [30,36,76,77]. In each time step, we compute the distance of Ti relative to Ba and O1 along the [001] direction and present the statistics of the distance in Fig. 4.

Figures 4(a)–4(c) and 4(d)–4(f) are the density distributions of Ti with respect to the position of Ba and O1 atoms, respectively, at different temperatures. The origin point of the abscissa is the center of two nearest neighbor Ba and O1 atoms in the [001] direction. For the distribution of Ti relative to Ba, all figures show a single-peaked distribution. In the low-temperature ferroelectric phase, as displayed in Fig. 4(a), Ti atoms tend to stay at one side and the peak deviates from the center by about 0.05 Å. However, as shown in Figs. 4(b) and 4(c) the distribution becomes symmetric with respect to the center when the temperature rises above the transition point. The distributions of Ti relative to O1 atoms are quite similar to those relative to Ba atoms, except that the tops of the peaks are flatter, as shown in Figs. 4(d)–4(f). Compared with the results of perturbative calculation [30] and molecular dynamics simulations based on model interactions [77], which yielded a double-peak distribution of Ti with respect to O atoms in the cubic phase, the FPMD results in Figs. 4(d)–4(f) show that the anharmonicity in the interaction between Ti and O atoms may be much smaller than previously estimated.

The anharmonicity in the interaction is illustrated by comparing the density distribution with a standard Gaussian distribution. Note that, when interactions between ions are all harmonic, the density distribution of an ion around its equilibrium position can be proved to be a Gaussian distribution [78]. Dotted lines in Fig. 4 represent the best Gaussian fit to the calculated Ti distribution. It shows that at all temperatures, the distributions of Ti relative to Ba almost coincide with
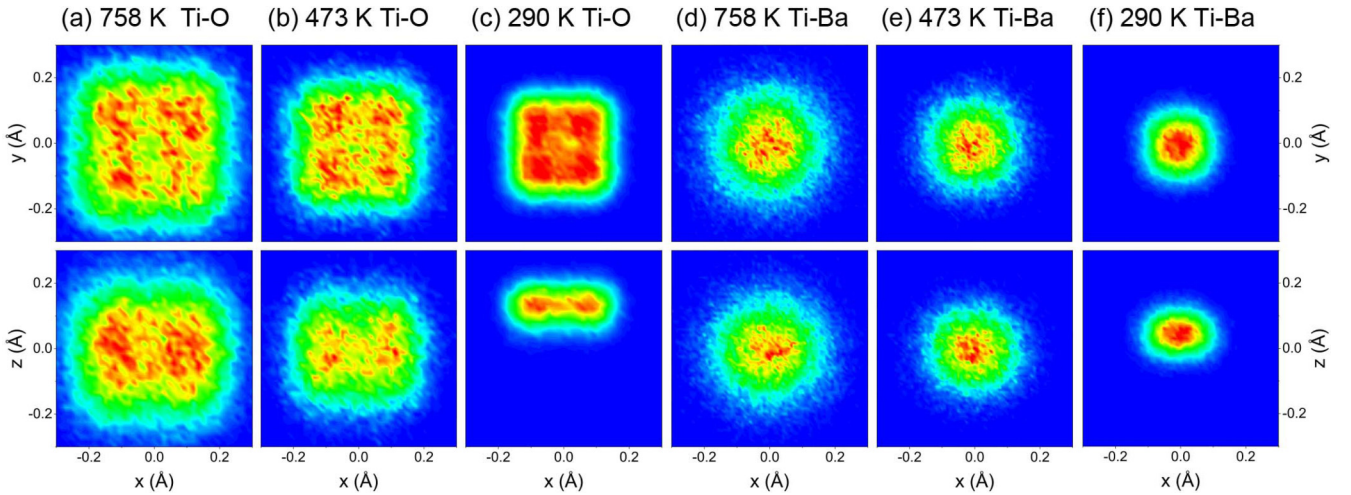
FIG. 5. Density distribution profiles of Ti in selected planes. (a), (b), and (c) are the distribution profile of Ti relative to O at 290 K, 473 K, and 758 K, respectively. (d), (e), and (f) are the Ti distribution relative to Ba at 290 K, 473 K, and 758 K, respectively. The first row is distributions in the $x-y$ plane, and the second row is those in the $x-z$ plane. Note that at 290 K, the $x-y$ plane for Ti-Ba distribution is at $z = 0.05$ Å. and the $x-y$ plane for Ti-O distribution is at $z = 0.12$ Å.

Gaussian distributions, suggesting that the anharmonicity in the Ti-Ba interaction is quite small and may be neglected in future Ti-Ba interaction models. In contrast, the distributions of Ti relative to O1 atoms at 473 K and 758 K display observable deviations from the Gaussian distributions, indicating non-negligible anharmonic interactions between Ti and O atoms in the cubic phase.

Details of the anharmonicity in the Ti-O interaction are further revealed in three-dimensional density distributions of Ti with respect to O atoms. As defined in Fig. 1, the [001] direction of BaTiO$_3$ is set along the z axis, and the perpendicular plane is the $x-y$ plane. Figures 5(a)–5(c) show the density distributions of Ti relative to the O octahedron in the $x-y$ and $x-z$ planes at selected temperatures, where the origin point of the coordinates system is the center of the octahedron. As a comparison, the density distributions of Ti with respect to the Ba cube in the same planes are displayed in Figs. 5(d)–5(f), where the origin point is placed at the center of the Ba cube.

In the BaTiO$_3$ cubic phase at 758 K and 473 K, as shown in Figs. 4(a) and 4(b), the distributions of Ti relative to the center of O octahedron in the $x-y$ and $y-z$ planes approximately have a square shape, while the distributions of Ti with respect to Ba cubic center are isotropic circular, as shown in Figs. 4(d) and 4(e). In addition, there is a squarelike region (which is the intersection of an approximately cubic region in three dimensions) near the center, inside which the distributions of Ti with respect to O are quite flat. This is very similar to the experimental result of Levin et al. [79].

In the cubic phase, the distributions of Ti with respect to Ba are well described by two-dimensional Gaussian distributions with negligible deviations, as revealed by a two-dimensional Gaussian fitting to the distributions, while the deviation in the distributions of Ti with respect to O from Gaussian distributions is easy to see from the squarelike shape and their flat distributions near the center. In the tetragonal phase, the distribution of Ti relative to O in the $x-z$ plane shows that Ti deviates from the center to one side in the [001] direction,

and its motion is constrained in a narrow long region near $z = 0.12$ Å, as shown in Fig. 5(c). However, the distribution of Ti relative to O in the $x-y$ plane at $z = 0.12$ Å shows that the square shape is still retained in the plane.

Flat-top distribution was interpreted as the superposition of a Gaussian distribution at the center and a multipeaked distribution by Qi et al. [36], and considered as a feature of the coexistence of displacive and order-disorder phase transition. However, a more straightforward interpretation is that it is a multidimensional super-Gaussian distribution [80]. In one dimension, the super-Gaussian function has a form of $\exp[-(|r|/a)^n]$, where r is the position, a is a scaling constant, and n is a number greater than 2. The flat-top distributions in Figs. 5(a) and 5(b) are thus well represented by a two-dimensional super-Gaussian function $\exp[-(|x_1|/a)^n]\exp[-(|x_2|/a)^n]$, with x_1 and x_2 two different coordinate components. In general, a distribution of an equilibrium system in coordinate space is proportional to $\exp[-U(\mathbf{r})/k_B T]$ following the Boltzmann distribution, where $U(\mathbf{r})$ is the effective potential at a given point $\mathbf{r}$, k_B is the Boltzmann constant, and T is the temperature. So, a super-Gaussian distribution suggests that the harmonic term in the potential is vanishing or very small. In addition, Fig. 5 also shows that the flat-top feature is essentially not affected by the temperature, implying that the vanishing of the harmonic interaction between Ti and O atoms is an intrinsic property of the cubic phase. Since the vanishing of harmonic interactions (not only near the transition point but all through the cubic phase) is quite unusual in a second-order phase transition, these findings may suggest an alternative mechanism in addition to the displacive and order-disorder types.

IV. SUMMARY

In summary, we have applied the full version of autocorrelation function method, i.e., the one together with the FPMD methods, to compute phonon dispersion of BaTiO$_3$ along

the [001] direction, as a typical example to illustrate subtle finite-temperature effects of phonons in entropy-stabilized structures. We show that the anharmonicity which leads to the strong smearing and damping of the longitudinal optical phonons mainly originates from the interaction between Ti and O atoms, as illustrated by the nearly constant density distribution of Ti relative to O atoms in a cubic region around the equilibrium position.

Our results suggest a further examination in future experiments for the theoretical results of the strong damping and smearing in the longitudinal optical modes and the temperature-dependent shift of the transverse optical modes in the TO1 branch. This may help to provide an improved theoretical model of ionic motion for entropy-stabilized structures. In addition, the subtle and rich phonon features caused by strong anharmonicity afford an important and critical benchmark reference for the upcoming machine-learning based molecular dynamics method used for the investigation of phonon properties.

APPENDIX: VIBRATIONAL MODES DECOMPOSITION

Vibrational motion can be analyzed using two decomposition methods. When the polarization vector of a given mode is known *a priori* or calculated using the DFPT method, one can project atomic displacements or velocities on the polarization vector following the method of Zhang *et al.* [47], which gives the information of energy and lifetime of the given mode. In parallel, the vibrational pattern can also be extracted using a filtering technique without the knowledge of polarization vectors.

The process to get atomic motions in a small frequency interval centered at ω_0 is as follows. Fourier transform of the time sequence of displacements is first conducted for each atom. Following that, the selected frequency is extracted through an ideal-(square)band-pass filter with a small frequency window, e.g., 1 THz as we used, and then the selected frequency sequence is transformed back to the time zone. Finally, add the obtained displacement to the equilibrium position of each atom to get the time sequence of trajectories, which can be displayed or used for further analyses.

It is relatively simple to get atomic motions associated to a given wave vector $\boldsymbol{q}$. First, the atomic motion in the supercell is projected into the small primitive cell following $\bar{\boldsymbol{u}}(^{1}_{b};t) = \frac{1}{N}\sum_{n}\boldsymbol{u}(^{n}_{b};t)\exp[-i\boldsymbol{q}\cdot\boldsymbol{r}(^{n}_{0})]$. Then, it is recovered as $\bar{\boldsymbol{u}}(^{n}_{b};t) = \bar{\boldsymbol{u}}(^{1}_{b};t)\exp[i\boldsymbol{q}\cdot\boldsymbol{r}(^{n}_{0})]$. Combining the filters in the frequency and wave vector spaces, the motion of given modes can be obtained.

[1] M. Born and K. Huang, *Dynamical Theory of Crystal Lattices*, International series of monographs on physics (Clarendon Press, Oxford, 1954).

[2] M. T. Dove, *Introduction to Lattice Dynamics*, Cambridge Topics in Mineral Physics and Chemistry (Cambridge University Press, Cambridge, 1993).

[3] R. Mittal, M. K. Gupta, and S. L. Chaplot, Prog. Mater. Sci **92**, 360 (2018).

[4] B. Fultz, Prog. Mater. Sci **55**, 247 (2010).

[5] H. J. Goldsmid, *Introduction to Thermoelectricity* (Springer, Berlin, Heidelberg, 2010).

[6] J. Bardeen, L. N. Cooper, and J. R. Schrieffer, Phys. Rev. **108**, 1175 (1957).

[7] M. Tinkham, *Introduction to Superconductivity*, 2nd ed. (Dover Publications, New York, 2004).

[8] W. Cochran, Phys. Rev. Lett. **3**, 412 (1959).

[9] N. W. Ashcroft and N. D. Mermin, *Solid State Physics* (Holt-Saunders, Philadelphia, 1976).

[10] P. J. Larkin, *Infrared and Raman Spectroscopy: Principles and Spectral Interpretation* (Elsevier, Amsterdam, 2018).

[11] P. R. G. Derek J. Gardiner, *Practical Raman Spectroscopy* (Springer, Berlin, Heidelberg, 1989).

[12] G. Shirane, Rev. Mod. Phys. **46**, 437 (1974).

[13] E. Burkel, Rep. Prog. Phys **63**, 171 (2000).

[14] G. Kresse, J. Furthmüller, and J. Hafner, Europhys. Lett. **32**, 729 (1995).

[15] K. Parlinski, Z. Q. Li, and Y. Kawazoe, Phys. Rev. Lett. **78**, 4063 (1997).

[16] S. Baroni, S. de Gironcoli, A. Dal Corso, and P. Giannozzi, Rev. Mod. Phys. **73**, 515 (2001).

[17] X. Gonze and C. Lee, Phys. Rev. B **55**, 10355 (1997).

[18] S. de Gironcoli, Phys. Rev. B **51**, 6773 (1995).

[19] A. Dal Corso and S. de Gironcoli, Phys. Rev. B **62**, 273 (2000).

[20] P. Giannozzi, S. de Gironcoli, P. Pavone, and S. Baroni, Phys. Rev. B **43**, 7231 (1991).

[21] A. Dal Corso, S. Baroni, R. Resta, and S. de Gironcoli, Phys. Rev. B **47**, 3588 (1993).

[22] Y. Zhao, Kun Ting Eddie Chua, C. K. Gan, J. Zhang, B. Peng, Z. Peng, and Q. Xiong, Phys. Rev. B **84**, 205330 (2011).

[23] O. Dubay and G. Kresse, Phys. Rev. B **67**, 035401 (2003).

[24] D. He, S. Buyukdagli, and B. Hu, Phys. Rev. E **78**, 061103 (2008).

[25] C. Zhang, C. Zhang, M. Chen, W. Kang, Z. Gu, J. Zhao, C. Liu, C. Sun, and P. Zhang, Phys. Rev. B **98**, 144301 (2018).

[26] Y. Lu, F. Zheng, W. Yang, W. Kang, Z. Li, C. Wang, Z. Gu, F. Tan, J. Zhao, C. Liu, C. Sun, and P. Zhang, J. Phys.: Condens. Matter **32**, 405404 (2020).

[27] M. T. Dove, Am. Mineral **82**, 213 (1997).

[28] H. Kay and P. Vousden, London, Edinburgh Dublin Philos. Mag. J. Sci. **40**, 1019 (1949).

[29] Y. Luspin, J. L. Servoin, and F. Gervais, J. Phys., C, Solid State Phys. **13**, 3761 (1980).

[30] Z.-X. Chen, Y. Chen, and Y.-S. Jiang, J. Phys. Chem. B **105**, 5766 (2001).

[31] R. A. Cowley, Phys. Rev. Lett. **9**, 159 (1962).

[32] C. LaSota, C.-Z. Wang, R. Yu, and H. Krakauer, AIP Conf. Proc. **436**, 139 (1998).

[33] B. Zalar, V. V. Laguta, and R. Blinc, Phys. Rev. Lett. **90**, 037601 (2003).

[34] E. A. Stern, Phys. Rev. Lett. **93**, 037601 (2004).

[35] J. Hlinka, T. Ostapchuk, D. Nuzhnyy, J. Petzelt, P. Kuzel, C. Kadlec, P. Vanek, I. Ponomareva, and L. Bellaiche, Phys. Rev. Lett. **101**, 167402 (2008).

[36] Y. Qi, S. Liu, I. Grinberg, and A. M. Rappe, Phys. Rev. B **94**, 134308 (2016).

[37] S. Ehsan, M. Arrigoni, G. K. H. Madsen, P. Blaha, and A. Tröster, Phys. Rev. B **103**, 094108 (2021).

[38] M. Paściak, T. R. Welberry, J. Kulda, S. Leoni, and J. Hlinka, Phys. Rev. Lett. **120**, 167601 (2018).

[39] M. S. Senn, D. A. Keen, T. C. A. Lucas, J. A. Hriljac, and A. L. Goodwin, Phys. Rev. Lett. **116**, 207602 (2016).

[40] J. M. Dickey and A. Paskin, Phys. Rev. **188**, 1407 (1969).

[41] J. A. Thomas, J. E. Turney, R. M. Iutzi, C. H. Amon, and A. J. H. McGaughey, Phys. Rev. B **81**, 081411(R) (2010).

[42] R. N. Barnett, U. Landman, A. Nitzan, and G. Rajagopal, J. Chem. Phys **94**, 608 (1991).

[43] P. Hohenberg and W. Kohn, Phys. Rev. **136**, B864 (1964).

[44] W. Kohn and L. J. Sham, Phys. Rev. **140**, A1133 (1965).

[45] R. Su, Z. Yuan, J. Wang, and Z. Zheng, J. Phys. A **49**, 255003 (2016).

[46] T. Lan, X. Tang, and B. Fultz, Phys. Rev. B **85**, 094305 (2012).

[47] D.-B. Zhang, T. Sun, and R. M. Wentzcovitch, Phys. Rev. Lett. **112**, 058501 (2014).

[48] Y. Lu, F.-w. Zheng, Y. Yang, P. Zhang, and D.-B. Zhang, Phys. Rev. B **100**, 054304 (2019).

[49] R. Car and M. Parrinello, Phys. Rev. Lett. **60**, 204 (1988).

[50] P. Vashishta, R. K. Kalia, and I. Ebbsjö, Phys. Rev. B **39**, 6034 (1989).

[51] H. Bao, B. Qiu, Y. Zhang, and X. Ruan, J. Quant. Spectrosc. Radiat. Transfer **113**, 1683 (2012).

[52] N. de Koker, Phys. Rev. Lett. **103**, 125902 (2009).

[53] G. Shirane, B. C. Frazer, V. J. Minkiewicz, J. A. Leake, and A. Linz, Phys. Rev. Lett. **19**, 234 (1967).

[54] J. Bouillot, C. Escribe, W. Fitzgerald, and L. Gnininvi, Solid State Commun. **30**, 521 (1979).

[55] B. Jannot, C. Escribe-Filippini, and J. Bouillot, J. Phys., C, Solid State Phys. **17**, 1329 (1984).

[56] J. Harada, J. D. Axe, and G. Shirane, Phys. Rev. B **4**, 155 (1971).

[57] D. Lu, H. Wang, M. Chen, L. Lin, R. Car, W. E, W. Jia, and L. Zhang, Comput. Phys. Commun **259**, 107624 (2021).

[58] X. Qian and R. Yang, Phys. Rev. B **98**, 224108 (2018).

[59] V. Ladygin, P. Korotaev, A. Yanilkin, and A. Shapeev, Comput. Mater. Sci. **172**, 109333 (2020).

[60] C. Chatfield, *The Analysis of Time Series: An Introduction*, 6th ed. (Chapman & Hall/CRC, Boca Raton, 2003).

[61] S. Tinte, M. Stachiotti, M. Sepliarsky, R. Migoni, and C. Rodriguez, Ferroelectrics **237**, 41 (2000).

[62] P. Giannozzi, S. Baroni, N. Bonini, M. Calandra, R. Car, C. Cavazzoni, D. Ceresoli, G. L. Chiarotti, M. Cococcioni, I. Dabo, A. D. Corso, S. de Gironcoli, S. Fabris, G. Fratesi, R. Gebauer, U. Gerstmann, C. Gougoussis, A. Kokalj, M. Lazzeri, L. Martin-Samos, N. Marzari, F. Mauri, R. Mazzarello, S. Paolini, A. Pasquarello, L. Paulatto, C. Sbraccia, S. Scandolo, G. Sclauzero, A. P. Seitsonen, A. Smogunov, P. Umari, and R. M. Wentzcovitch, J. Phys.: Condens. Matter **21**, 395502 (2009).

[63] P. E. Blöchl, Phys. Rev. B **50**, 17953 (1994).

[64] R. O. Jones and O. Gunnarsson, Rev. Mod. Phys. **61**, 689 (1989).

[65] G. H. Kwei, A. C. Lawson, S. J. L. Billinge, and S. W. Cheong, J. Phys. Chem. **97**, 2368 (1993).

[66] H. D. Megaw, Trans. Faraday Soc. **42**, A224 (1946).

[67] J. A. Bland, Can. J. Phys. **37**, 417 (1959).

[68] W. Zhong, D. Vanderbilt, and K. M. Rabe, Phys. Rev. B **52**, 6301 (1995).

[69] W. Zhong, D. Vanderbilt, and K. M. Rabe, Phys. Rev. Lett. **73**, 1861 (1994).

[70] Y. Zhang, J. Sun, J. P. Perdew, and X. Wu, Phys. Rev. B **96**, 035143 (2017).

[71] J. P. Perdew, K. Burke, and M. Ernzerhof, Phys. Rev. Lett. **77**, 3865 (1996).

[72] J. Sun, A. Ruzsinszky, and J. P. Perdew, Phys. Rev. Lett. **115**, 036402 (2015).

[73] N. Marzari and D. Vanderbilt, Phys. Rev. B **56**, 12847 (1997).

[74] M. Stengel and N. A. Spaldin, Phys. Rev. B **73**, 075121 (2006).

[75] H. H. Wieder, Phys. Rev. **99**, 1161 (1955).

[76] M. J. Noordhoek, V. Krayzman, A. Chernatynskiy, S. R. Phillpot, and I. Levin, Appl. Phys. Lett. **103**, 022909 (2013).

[77] N. L. Matsko, E. G. Maksimov, and S. V. Lepeshkin, J. Exp. Theor. Phys. **115**, 309 (2012).

[78] This is easy to see if one notices that the joint distribution with respect to all ions is a multidimensional Gaussian distribution for harmonic interactions. When the coordinates of other ions are integrated out, the one-particle distribution for the ion of interest is a three-dimensional Gaussian distribution. Its projection in a given direction is a one-dimensional Gaussian distribution.

[79] I. Levin, V. Krayzman, and J. C. Woicik, Phys. Rev. B **89**, 024106 (2014).

[80] M. Santarsiero and R. Borghi, J. Opt. Soc. Am. A **16**, 188 (1999).